EXTENSIONAL FLOW OF ERYTHROCYTE MEMBRANE FROM CELL BODY TO ELASTIC TETHER

I. Analysis

R. M. HOCHMUTH AND E. A. EVANS

Department of Biomedical Engineering, Duke University, Durham, North Carolina 27706

ABSTRACT   This is the first of two papers on an analytical and experimental study of the flow of the erythrocyte membrane. In the experiment to be discussed in detail in the second paper, preswollen human erythrocytes are sphered by aspirating a portion of the cell membrane into a small micropipette; and long, thin, membrane filaments or "tethers" are steadily withdrawn from the cell at a point diametrically opposite to the point of aspiration. The aspirated portion of the membrane furnishes a "reservoir" of material that replaces the membrane as it flows as a liquid from the nearly spherical cell body to the cylindrical tether. In this paper we show that an application of the principle of conservation of mass permits the tether radius (~200 Å or less) to be measured with the light microscope as the tether is formed and extended at a constant rate. A static analysis of the axisymmetric cell deformation and tether formation process reveals that the tether radius is uniquely determined by the isotropic tension in the membrane and the elastic constitutive (material) behavior of the tether itself. A dynamic analysis of the extensional flow process reveals that the tether radius must decrease as the velocity of the tether is increased and that the decrease depends on both the viscosity of the membrane and the elasticity of the tether. The analysis also shows that these two factors (membrane viscosity and tether elasticity) are readily decomposed and determined separately when flow experiments are performed at different isotropic tensions.

INTRODUCTION

Recognition that a lipid bilayer is a major structural component of biomembranes has led to the view that a membrane has a liquidlike character. Usually, the liquid nature of the membrane is pictured in terms of "local" or molecular phenomena such as the lateral or rotational motion of specific molecular marker particles surrounded by the long-chain polar hydrocarbons of the planar bilayer. Ultimately, however, if a membrane is liquidlike then it must flow as a continuum. That is, as long as the membrane is not geometrically constrained in some way, an observable deformation and rate of deformation must occur when an external force acts on the membrane. Such studies of the macroscopic flow behavior of membrane when characterized by an appropriate constitutive relation will lead to measurements of the surface viscosity of living membrane.

In the analysis presented here, an axisymmetric geometrical situation has been created to produce extensional flow of membrane when acted on by an external force. As shown in Fig. 1, a swollen but initially nonspherical erythrocyte is aspirated into a pipette until the cell forms a

sphere that is outside the pipette and a membrane tongue (a cylinder with hemispherical cap) within the pipette (Rand and Burton, 1964; Evans et al., 1976). At a point on the erythrocyte opposite to the point of aspiration, a small spherical bead has been allowed to adhere to the membrane. The bead, in turn, is held by a second pipette with a strong aspiration pressure. When the second pipette is withdrawn at a constant rate with an electromechanical linear translator, a long, thin, apparently hollow membrane cylinder or "tether" is extracted from the spherical cell body (Hochmuth et al., 1982).

The formation of the tether is anticipated, since tethers have been extracted from flaccid erythrocytes that were allowed to adhere to a glass surface and were subsequently acted on by a fluid shear force (Hochmuth et al., 1973; 1976). However, in the original tether experiments of Hochmuth et al. (1973) the excess surface area for the tether comes from the surface of a flaccid erythrocyte. In the experiments analyzed here, even though the cell body is essentially a sphere, an excess of membrane for the tether is readily supplied by a reservoir of material in the pipette. The recognition of this fact leads to a method for measurement of the tether radius during the process of tether formation.

In our analysis of the original tether-flow experiments (Evans and Hochmuth, 1976), we assumed an axisymmet-
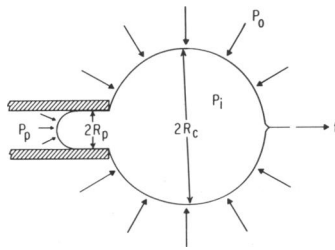

FIGURE 1 Line drawing depicting the aspiration of a preswollen cell into a pipette until it forms a sphere, and subsequent extraction of a thin membrane filament or tether. P_p, pipette pressure; P_o, reservoir (outside) pressure; P_i, internal hydrostatic pressure; f, external force on the tether; R_p, pipette radius; and R_c, maximum cell radius (at the equator).

ric configuration as an approximation of the true and quite complicated cell geometry. In the present situation depicted in Fig. 1, both analysis and experiment are geometrically congruent.

The idealized model of the membrane flow process to be analyzed here is shown in Fig. 2. The membrane enclosing the cell body is modeled as a liquid. The liquid membrane flows at a constant rate onto a tether which translates as a rigid body. The tether is modeled as an elastic solid; i.e., it will elongate in response to an increasing force. Three conditions are satisfied at the junction of the liquid membrane and the elastic tether: (a) The velocity is continuous; i.e., the velocity of the membrane equals the velocity of the tether. (b) The rate of deformation is continuous and equal to zero for both membrane and tether. (c) The axial forces are equal; i.e., the meridional tension in the membrane times the circumference of the membrane at the point where it joins the tether is equal to the net axial force acting on the tether.

An analysis of the model illustrated by Fig. 2 predicts that larger positive flow rates produce small tether radii and that larger negative flow rates, when the tether flows onto the cell, produce larger tether radii. As we will show, these analytic predictions agree with experimental observations and, also, permit the experimental data to be "collapsed" onto a single curve. Thus we propose the model illustrated in Fig. 2 as the simplest one we can formulate that predicts and describes the experiments. However, there are certain assumptions implicit in the model that are

only correct in an approximate sense. In particular, we have assumed that the liquid membrane enclosing the cell body is very thin in comparison to the radius of the tether. In reality, the thickness of the membrane relative to the tether radius can be significant. For an analysis of the flow of a thick membrane we would have to define local azimuthal and meridional stresses (forces per area) rather than tensions (forces per length). Such membrane stresses would equal the axial and circumferential stresses in the tether at the point where the membrane of the cell body flows into the tether. In addition, it may be necessary to treat the thick membrane as a multicomponent lamellar structure with viscous slip between adjacent layers and, possibly, a bending resistance within a given layer and between adjacent layers. Clearly, such a model would be one of great complexity with several elastic and viscous constants. On the other hand, the idealized model represented by Fig. 2 characterizes the flow of the membrane with a single viscous coefficient, and the analytical predictions of the basic model agree closely with experimental observations (Hochmuth et al., 1982).

STATIC DEFORMATION

The membrane of a sphered and tethered erythrocyte which is held in a pipette (Fig. 1) is acted upon by various pressures and forces: a tether force f, an outside pressure in the reservoir P_o, an aspiration pressure in the pipette P_p, an internal pressure P_i, and a force resultant (not shown) between the cell membrane and the pipette wall. To determine how these forces interact with each other and, in so doing, specify the equilibrium shape of the erythrocyte, a free-body diagram is created by making a cut through the cell membrane with a plane that is perpendicular to the z-axis of symmetry (Fig. 3). By making such a cut, the internal force resultants or tensions in the membrane are revealed. The membrane tension $\bar{T}$ shown in Fig. 3 is assumed to be isotropic as though the membrane were a two-dimensional liquid. For the erythrocyte membrane, which has a definite surface shear rigidity (Evans, 1973), this assumption is appropriate as long as the cell has been pulled with a strong aspiration pressure into a spherical or nearly spherical shape. In particular since the erythrocyte
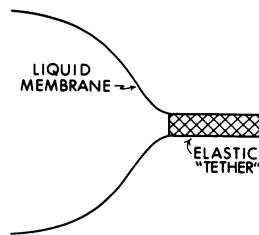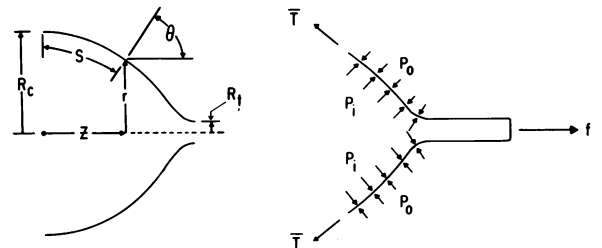

FIGURE 2 Model of the membrane flow process. The liquid membrane of the erythrocyte flows onto an elastic tether. A change in the force on the tether produces an elastic response of the tether and a viscous response of the membrane.

FIGURE 3 Intrinsic coordinate system and free body diagram of the cell body. s, r, z are meridional, radial, and axial coordinates; θ, angle between outward normal and horizontal; ϕ, circumferential angle; R_t, tether radius; and $\bar{T}$, isotropic tension in the membrane.

membrane has a surface elastic shear modulus of 0.006 dyn/cm (Waugh and Evans, 1979), membrane tensions on the order of 0.1 dyn/cm or greater (which correspond to aspiration pressures of ~0.001 atm or greater) permit the erythrocyte membrane to be treated as a two-dimensional liquid.

This "liquid-membrane assumption" together with the equation of membrane equilibrium along the meridian s ($d\overline{T}/ds = 0$) implies that $\overline{T}$ is constant everywhere in the membrane as long as there is no net flow in the membrane or no external fluid flow over the surface of the membrane. Thus, a force balance in the z direction (which is essentially an integration of the law of Laplace for the situation shown in Fig. 3) immediately yields:

$$(\overline{T}\sin\theta)\, 2\pi r = (\Delta P)_w \pi r^2 + f^0 \tag{1}$$

where f^0 is the static tether force (the tether force at zero velocity), θ is the angle between the outward normal and the horizontal, and the wall pressure difference, $\Delta P_w = P_i - P_o$. A series of cuts through the pipette, tether, and cell body at its maximum radius gives the following expression:

$$(\Delta P)_w = \frac{(\Delta P)\dfrac{R_p}{R_c} - \dfrac{f^0}{\pi R_c^2}}{1 - R_p/R_c} \approx \frac{(\Delta P)\dfrac{R_p}{R_c}}{1 - R_p/R_c}$$

and

$$\overline{T} \approx \frac{(\Delta P)R_p/2}{1 - R_p/R_c}, \tag{2}$$

where ΔP is the overall pressure difference ($\Delta P = P_o - P_p$; Fig. 1). The tether-force term, $f^0/\pi R_c^2$, can be neglected in the calculation of $(\Delta P)_w$ and $\overline{T}$ from the experimental measurements of ΔP, R_p and R_c since the force term is several orders of magnitude less than the overall pressure-difference term for all cases analyzed here.

Eq. 1 can be arbitrarily, but conveniently, scaled with respect to the maximum cell radius R_c. Thus, let $\tilde{r} = r/R_c$, $\tilde{f}_w^0 = f^0(\Delta P)_w \cdot \pi R_c^2$ and evaluate $\overline{T}$ at $r = R_c(\theta = \pi/2)$:

$$\sin\theta = \frac{\tilde{r} + \tilde{f}_w^0\, \tilde{r}}{1 + \tilde{f}_w^0}. \tag{3}$$

Eq. 3 has the essential features of the geometry of the cell and reveals a very important fact: viz, the existence of the tether. For as long as f is finite (if $f = 0$, then Eq. 3 is just the equation for a spherical surface), Eq. 3 admits two solutions for $\tilde{r}$ when $\theta = \pi/2$ (when the surface is tangential to the horizontal). The obvious solution is $\tilde{r} = 1$ ($r = R_c$) at $\theta = \pi/2$. However, as $\tilde{r}$ decreases, the membrane will eventually turn the corner and $\theta \rightarrow \pi/2$ as $\tilde{r} \rightarrow \tilde{f}_w^0$. This means that the cell forms a tether at this point and the radius of the tether, $r = R_t^0$, is given by $\tilde{R}_t^0 = \tilde{f}_w^0$ or

$$\frac{R_t^0}{R_c} = \frac{f^0}{(\Delta P)_w \pi R_c^2}.$$

In dimensional form,

$$R_t^0 = \frac{f^0}{\Delta P_w \pi R_c} = \frac{f^0}{2\pi\overline{T} - f/R_c} \approx \frac{f^0}{2\pi\overline{T}}. \tag{4}$$

In all cases analyzed here, $\overline{T} \gg f^0/2\pi R_c$ and, thus, the cell surface is essentially spherical except in a small region near the tether (Fig. 1).[1] Eq. 4 reveals that the characteristic dimension in this problem is given by the ratio of the tether force to the isotropic tension. The geometric dimensions of pipette radius R_p and cell radius R_c are used to calculate the isotropic tension in the membrane from a measurement of the pressure difference (Eq. 2). However, under static conditions the tether radius depends only on the force on the tether and the isotropic tension in the membrane as indicated by Eq. 4.

At first glance, Eq. 4 appears to indicate that the tether problem is not unique. That is, for a given $\overline{T}$ (i.e., a given aspiration pressure ΔP, Eq. 2) there exists an infinite number of tether radii depending on the value for f. However, experimental observations of tethered cells reveal that this is not the case (Hochmuth et al., 1982). At a relatively low tension the cell body is somewhat elongated in the z direction and the tether appears as a faint shadow, stretched between the cell body and its point of attachment. At higher tensions the cell assumes a more nearly spherical shape and the tether disappears since its diffraction pattern becomes unobservable. Lowering the tension (pressure) reveals the tether again as a faint shadow and creates an elongated cell body. It appears that the tether radius is a function of the tension in the membrane and, thus, that the tether radius depends on the tether force according to Eq. 4. That is, the tether has elastic behavior, in contrast to the rest of the cell membrane which is modeled as a liquid since the isotropic tension in the membrane is much greater than the shear modulus. Tethers of relatively large radii (~0.1 μm) in the flow-channel experiments of Hochmuth et al. (1973) were also observed to have this elastic behavior. With this assumption of elastic constitutive behavior, $f = f(R_t)$; that is, the tether force is a unique function of the tether radius. Since $\overline{T}$ is imposed in the experiment and since R_t can be measured, as discussed in the next section, then the elastic behavior of the tether, $f = f(R_t)$, can be determined in principle from Eq. 4. Intuitively, it is expected that the tether force will be inversely related to the tether radius and, in fact, the original observations of Hochmuth et al. (1973) for relatively large tethers indicate this is the case.

In general, the static shape of the cell can be obtained from Eq. 1 along with various equations from differential geometry (those which relate r, θ, s, and z) and two

---

[1] The work of Hochmuth et al. (1973) with flaccid erythrocytes indicates a tether force on the order of 10^{-6} dyn. In the present work the tether force is on the order of the isotropic tension (~0.3 dyn/cm) times the tether circumference (10^{-5} cm). Thus, the tether force still is on the order of 10^{-6} dyn. Since $\overline{T} \sim 0.3$ dyn/cm and $f^0/2\pi R_c \sim 10^{-3}$ dyn/cm ($R_c \sim 3$ μm), $\overline{T} \gg f^0/2\pi R_c$.
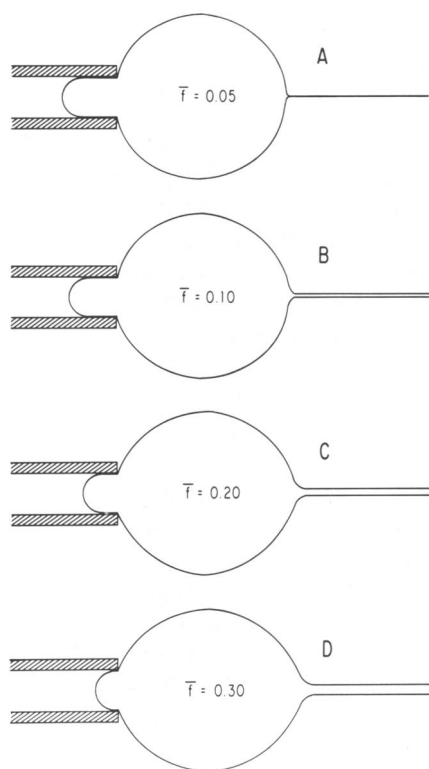
FIGURE 4 Results of the analysis of the static deformation of a tethered red cell at constant membrane surface area, constant internal volume and constant distance from pipette to the point of attachment of the tether. A–D illustrate the effect of an increase in the dimensionless tether force $\bar{f}$ ($\bar{f} = f/\Delta P \cdot \pi R_p^2$ where $\Delta P = P_o - P_p$: Fig. 1). Note the increase in the tether radius, the increased deformation of the cell body and the movement of the membrane "tongue" down the pipette as $\bar{f}$ is increased.

constraints: the total surface area and volume of the cell remain constant during the deformation process. The solution for the overall shape of the cell is discussed in detail in Appendix A. The results of one such numerical calculation are shown in Fig. 4. Here, $\bar{f}^0$ is a dimensionless force given by the tether force f scaled with respect to the overall suction pressure drop ΔP and the cross-sectional area of the pipette πR_p^2: $\bar{f}^0 = f^0/(\Delta P \cdot \pi R_p^2)$.[2] Fig. 4 shows that as the suction pressure is increased relative to the tether force (as $\bar{f}$ decreases), the tether becomes smaller and more material is aspirated into the pipette. (Compare Fig. 4 D to A). During this aspiration process, the overall surface area and volume are held constant, as is the distance from the origin of the tether to the mouth of the pipette. A particular case (Fig. 4 D where $\bar{f}$ = 0.3) is matched to an actual erythrocyte with tether as shown in Fig. 5. The match is not perfect since the erythrocyte is somewhat more elongated and its tether appears to be smaller than the relatively large tether in Fig. 4 D.

---

[2]After a certain amount of algebraic manipulation it can be shown that $\tilde{f}_w^0$ is given by $\tilde{f}_w^0 = (\bar{f}^0/\bar{R}_c)[(\bar{R}_c - 1)/(\bar{R}_c - \bar{f}^0)] \sim (\bar{f}^0/\bar{R}_c)$, where $\bar{R}_c = R_c/R_p, \tilde{f}_w^0 = f^0/(\Delta P_w \pi R_c^2)$, and $\bar{f}^0 = f^0/(\Delta P)\pi R_p^2$. Typically, $\tilde{f}_w^0$ is about one-third to one-fourth as large as $\bar{f}^0$.
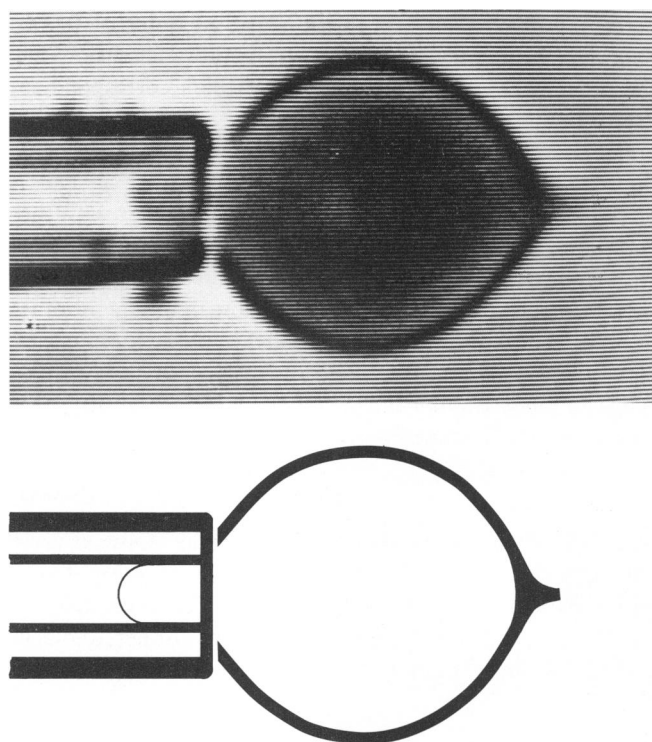

FIGURE 5 Comparison of a tethered erythroycte at a membrane tension ~0.1 dyn/cm with the particular result shown in Fig. 4 C.

TETHER RADIUS

At first thought it would seem to be almost impossible to measure *in situ* something as thin as a tether. However, the method of tether formation presented in this paper and depicted in Figs. 1, 4, and 5 permits the tether radius to be measured as the tether is being formed. In essence, a reservoir of membrane material is created within the pipette. As the tether is extracted from the cell body, the material in the reservoir is depleted. Since this process occurs at constant total surface area (the membrane surface area is constant at constant isotropic tension; Evans et al., 1976) and constant internal volume, it can be shown readily (Appendix B) that the decrease of material (surface area) within the pipette is essentially balanced by an increase in membrane material in the tether:

$$-2\pi R_p \, dL_p \qquad \approx \qquad 2\pi R_t \, dL_t$$

(Decrease of material   (Increase of material
in pipette)   in tether)

where $-dL_p$ is the decrease in length of the aspirated portion of the membrane within the pipette and dL_t is the increase in tether length. The solution of this equation for the unknown tether radius gives

$$R_t \approx R_p \cdot \left(-\frac{dL_p}{dL_t}\right). \qquad (5)$$

As shown in Appendix B the assumption of a spherical cell body of radius R_c allows Eq. 5 to be written as an

equality:

$$R_t = \left(1 - \frac{R_p}{R_c}\right) \cdot R_p \cdot \left(-\frac{dL_p}{dL_t}\right). \qquad (6)$$

As we show in our next paper (Hochmuth et al., 1982) Eq. 6 provides a means for the accurate measurement of the tether radius, even though the tether radius is less than the wavelength of light.

SCALE

For the problem of membrane flow from cell body to tether, there are essentially only three scaling parameters: a characteristic tether radius at zero velocity, R_t^0; a characteristic isotropic tension in the membrane, $\overline{T}$; and a membrane viscosity, η. The scaling of variables with respect to these three parameters is denoted by a circumflex (^). Thus, the dimensionless tether radius is $\hat{R}_t = R_t/R_t^0$. The dimensionless azimuthal and meridional tensions are $\hat{T}_\phi = T_\phi/\overline{T}$ and $\hat{T}_m = T_m/\overline{T}$. Since the tether force at zero velocity is $f^0 = 2\pi R_t^0 \overline{T}$ (see Eq. 4), the dimensionless tether force is $\hat{f} = f/f^0$. Finally, as we will show, the natural scale for the tether velocity V_t is $\hat{V}_t = 2\eta V_t/R_t^0 \overline{T}$.

MEMBRANE FLOW

In practice, tethers are formed at a finite rate and, thus, membrane material must flow continuously from cell body to tether as shown in Fig. 6. In this case the tension in the membrane is not constant but increases in the direction of flow (along the meridian s in Fig. 3) and produces a positive tension gradient.

To gain insight into the essential nature of the flow of membrane material from cell body to tether (Fig. 6), an approximate but relatively straightforward analysis of this flow problem is given here. Consider that the membrane material external to the tether forms a circular but flat sheet rather than the curved surface shown in Fig. 6. This sheet lies entirely in a plane perpendicular to the tether (z) axis. In this case, the equation of continuity (conservation of mass) immediately gives the velocity profile in the
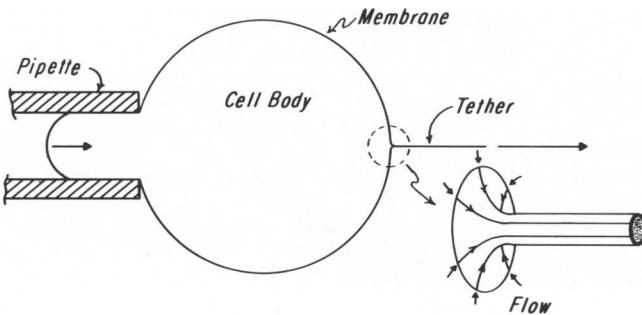

FIGURE 6 Illustration of the flow of membrane material from cell body to tether. Since mass is conserved, the membrane tongue moves slowly down the pipette as more membrane material flows onto the tether. The ratio of the rate of movement of material down the pipette to the velocity of the tether is proportional to the ratio of the radius of the tether to the radius of the pipette.

membrane material that flows onto the tether:

$$v_r = -\frac{V_t R_t}{r}, \qquad (7)$$

where r is the radial distance from the z axis, v_r is the velocity in the r direction and V_t is the tether velocity. There is a negative sign in Eq. 7 since v_r is positive in the positive r direction and V_t is positive in the positive z direction. Eq. 7 demonstrates that most of the flow occurs in a small region around the tether where $r \rightarrow R_t$.

In order to relate the local velocity field to local tensions in the membrane, a certain type of constitutive or material behavior must be assumed. The simplest or first-order linear approximation is that membrane material flow is governed by a Newton's law of viscosity relationship:

$$T_r = \overline{T} + 2\eta \frac{\partial v_r}{\partial r} \qquad (8)$$

where T_r is the tension in the radial direction and $\overline{T}$ is the isotropic tension in the far field where $\partial v_r/\partial r \rightarrow 0$. The isotropic tension $\overline{T}$ is imposed by the aspiration pressure ΔP and is readily calculated (Eq. 2).

The field equation for T_r is obtained by the substitution of Eq. 7 into 8:

$$T_r = \overline{T} + \frac{2\eta V_t R_t}{r^2}. \qquad (9)$$

The radial tension relative to the isotropic component increases rapidly as r decreases to its minimum value ($r \rightarrow R_t$).

Eq. 9 describes a sheet flowing into a cylinder (tether) which then translates as a rigid body in a direction perpendicular to the plane of the sheet (as long as R_t remains constant). At the circumferential line where the sheet joins the cylinder it is assumed that the radial tension is continuous. (In reality, the membrane material undergoes a continuous turning of the corner (Fig. 6) and the radial tension is, clearly, continuous along the entire arc length). Thus,

$$T_r|_{r-R_t} 2\pi R_t = f(R_t). \qquad (10)$$

Compare Eq. 10 to 4, where $V_t \rightarrow 0$, and note in the present case that the local radial tension is substituted for the isotropic tension.

The evaluation of Eq. 9 at $r = R_t$ and the substitution of Eq. 10 into 9 yields, after some algebraic manipulation,

$$R_t = \frac{f(R_t)}{2\pi \overline{T}} - \frac{2\eta V_t}{\overline{T}}. \qquad (11)$$

Eq. 11 is readily scaled by dividing both sides by the tether radius at zero velocity, R_t^0, and using the relationship given by Eq. 4:

$$\hat{R}_t = \hat{f} - \hat{V}_t, \qquad (12)$$

where $\hat{R}_t = R_t/R_t^0$, $\hat{f} = f/f^0$, and $\hat{V}_t = 2\eta V_t/R_t^0 \overline{T}$.

Eq. 11 shows that under the dynamic condition of flow, the tether radius depends on both the elastic constitutive behavior of the tether and the viscous behavior of the membrane surface as it flows onto (or off of) the tether. Also, it is important to note that the velocity term in Eq. 11 has a sign. That is, when a tether is being extracted from the erythrocyte, $V_t > 0$ and when the tether is being absorbed by the erythrocyte, $V_t < 0$. Thus,

$$R_t = \frac{f}{2\pi\overline{T}} + \frac{2\eta|V_t|}{\overline{T}}, \quad V_t \leq 0.$$

Eq. 11 is derived for an idealized flat-surface approximation to an actual curved surface as shown in Fig. 6. An analysis for a general curved surface involves the application of Newton's law of viscosity to the equations of membrane equilibrium in which there exists nonisotropic tensions along a principal axis system. This is essentially the approach taken in a previous study (Evans and Hochmuth, 1976) of the flow of membrane material from flaccid erythrocytes ($\Delta P \approx 0$, $\overline{T} \approx 0$ and f is produced by a fluid shear stress in a flow channel).[3] This more general analysis is discussed in Appendix C. A result of this analysis is shown in Fig. 7. Here, the solid lines show the numerical integration of the equations of membrane equilibrium and flow (Appendix C) for particular values of the tether force f relative to the force at zero velocity f^0: $\hat{f} = f/f^0$. The slope of these constant-force lines at the origin are shallower, by a factor of 1:1.6, than the $-45°$ slope predicted by Eq. 12. Thus, for Eq. 12 to agree with the numerical solution at the origin (as $\hat{V}_t \rightarrow 0$), Eq. 12 must be modified as follows:

$$\hat{R}_t = \hat{f} - \hat{V}_t/C \tag{13}$$

where $C \approx 1.6$.

The solid, constant-force lines shown in Fig. 7 do not model the experimental situation. Observations of Hochmuth et al. (1973, 1982) indicate that as the force on the elastic tether is increased, the tether radius will decrease. A simple first-order phenomenological expression (Hochmuth et al., 1982) that describes an inverse relation between force and radius is given by

$$\hat{f} = 1/\hat{R}_t. \tag{14}$$

For this particular case, the relation between the tether radius and the tether velocity is shown by the dashed line in Fig. 7. The slope of this line at the origin is exactly one-half that of the constant-force line.

The shape of the liquid membrane as it flows from the maximum cell radius to the tether is shown in Fig. 8 for the force-radius relation given by Eq. 14. (For the sake of illustration, we have chosen an abnormally large value of

---

[3]It is interesting to note for $\overline{T} = 0$, Eq. 11 reduces to $f = 4\pi\eta V_t$; thus the viscosity determination is independent of the radius of the tether, as first noted by Evans and Hochmuth (1976).
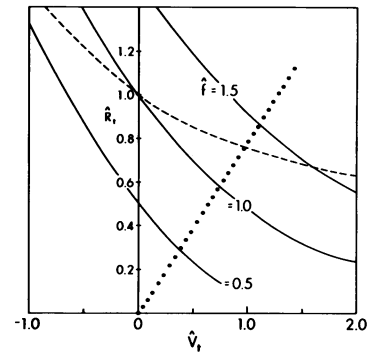

FIGURE 7 The solid lines denote the change in dimensionless tether radius with dimensionless tether velocity at different values of the dimensionless force. The slope of these lines at the origin is $\sim -1/1.6$. The dashed line is derived from a specific elastic relation between the dimensionless force and the dimensionless tether radius: $\hat{f} = 1/\hat{R}_t$. The results to the right of the dotted line through the origin produce an azimuthal tension, T_ϕ, which is negative. In this figure, $\hat{R}_t = R_t/R_t^0$, $\hat{f} = f/f^0$ and $\hat{V}_t = 2\eta V_t/\overline{T}R_t^0$ where the 0 superscript denotes the value at zero velocity ($R_t \rightarrow R_t^0$ and $f \rightarrow f^0 = 2\pi R_t^0\overline{T}$ as $V_t \rightarrow 0$).

0.1 for the ratio of the tether radius at zero velocity, R_t^0, to the cell radius R_c; i.e., $R_t^0/R_c = 0.1$. The results are slightly dependent on this ratio until it becomes about an order-of-magnitude smaller.) For the situation depicted in Fig. 8, the scaled local values of the meridional tension, $\hat{T}_m$, azimuthal tension, $\hat{T}_\phi$, and the fluid shear, $\partial\hat{v}_s/\partial\hat{s}$, are shown in Fig. 9. In terms of these scaled variables, Newton's law of viscosity is given by

$$\frac{\hat{T}_m - \hat{T}_\phi}{2} = \frac{\partial\hat{v}_s}{\partial\hat{s}} \tag{15}$$

where $\hat{T}_m = T_m/\overline{T}$, $\hat{T}_\phi = T_\phi/\overline{T}$, $\hat{v}_s = 2\eta v_s/R_t^0\overline{T}$ and $\hat{s} = s/R_t^0$. Since the maximum value for the dimensionless
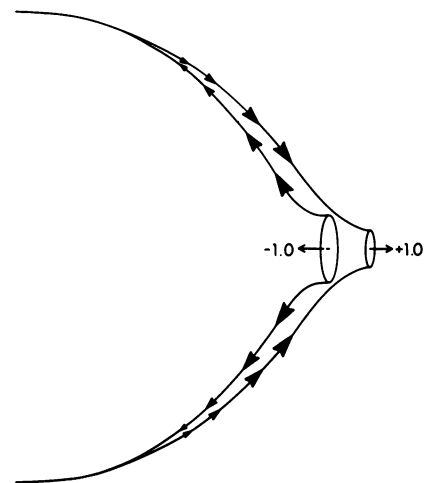

FIGURE 8 The shape of the liquid membrane at two different dimensionless tether velocities, $\hat{V}_t = \pm 1.0$ ($\hat{V}_t = 2\eta V_t/R_t^0\overline{T}$), for the force-radius relation given by Eq. 14. For the sake of illustration, the ratio of the tether radius at zero velocity, R_t^0, to the maximum cell radius, R_c, is set equal to 0.1. This value is about an order-of-magnitude larger than the experimental situation.

fluid shear shown in Fig. 9 is on the order of the dimensionless tether velocity, the maximum value for the dimensional fluid shear or shear rate will be on the order of the tether velocity divided by the tether radius.

As the tether velocity is increased, the minimum value for the azimuthal tension will decrease until it becomes negative; i.e., the membrane becomes loaded in compression in the azimuthal direction. (Note in Fig. 9 that the minimum value for $\hat{T}_\phi$ is almost zero when $\hat{V}_t = 1.0$). This compression in the azimuthal direction could lead to an unstable buckling or wrinkling of the membrane. Negative values for $\hat{T}_\phi$ exist in the region to the right of the dotted line through the origin of Fig. 7. However, few experiments are performed in this region since the tether either breaks or detaches at large values of $\hat{V}_t$.

In order to obtain an expression for the viscosity η, Eq. 13 in dimensional form is differentiated with respect to V_t at constant $\overline{T}$ and then rearranged:

$$\frac{2\eta}{C\overline{T}} = \left[\frac{1}{2\pi\overline{T}}\frac{df}{dR_t} - 1\right]\left(\frac{\partial R_t}{\partial V_t}\right)_{\overline{T}}. \tag{16}$$

The tether elasticity term can be evaluated at zero tether velocity where $f^0 = 2\pi R_t^0 \overline{T}$ (Eq. 4) and

$$\frac{df}{dR_t} = \frac{df^0}{dR_t^0}.$$

Eq. 16 provides the means for the measurement of tether viscosity. In order to make this measurement, both the change in tether radius with tether velocity and the tether elastic behavior, $f = f(R_t)$, must be known. In addition,
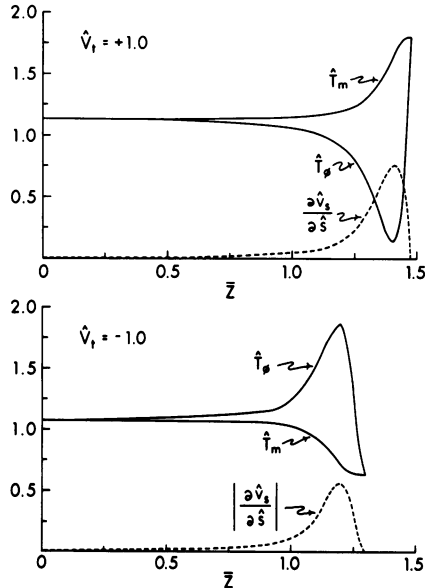

FIGURE 9 The dimensionless meridional tension, $\hat{T}_m$, azimuthal tension, $\hat{T}_\phi$, and viscous deviatoric component, $\partial v_s/\partial s$, for the geometry depicted in Fig. 8. ($\hat{T}_m = T_m/\overline{T}$, $\hat{T}_\phi = T_\phi/\overline{T}$, $\hat{v}_s = 2\eta v_s/R_t^0\overline{T}$, $\hat{s} = s/R_t^0$). The axial distance z is scaled with respect to the maximum cell radius: $\bar{z} = z/R_c$. Note that $T_m = T_\phi = \overline{T}$ at the beginning and end of the flow process.

Eq. 16 provides an estimate of the lower bound for the viscosity:

$$\eta > \left(\frac{C\overline{T}}{2}\right)\left(-\frac{\partial R_t}{\partial V_t}\right)_{\overline{T}}.$$

An alternate form of Eq. 16 which is slightly more useful in the calculation of a value for η can be obtained by expanding the tether-force term (Eq. 10) and evaluating it at the static state:

$$f = 2\pi R_t T_r|_{r=R_t}$$

$$\left(\frac{df}{dR_t}\right)_{R_t=R_t^0} = 2\pi R_t^0\frac{d\overline{T}}{dR_t^0} + 2\pi\overline{T}.$$

Thus, Eq. 16 becomes

$$\eta = \frac{C}{2}R_t^0\left(\frac{d\overline{T}}{dR_t^0}\right)\left(\frac{\partial R_t}{\partial V_t}\right)_{\overline{T}}. \tag{17}$$

In the paper to follow (Hochmuth et al., 1982), Eq. 17 will be used to calculate a value for the membrane surface viscosity η.

YIELD

The tether formation studies of Hochmuth et al. (1973) suggest that the erythrocyte membrane possesses a "yield", i.e., a point where the absolute value of the elastic shear resultant exceeds a certain critical value and the membrane begins to flow (Evans and Hochmuth, 1976). The yield shear resultant, T_y, represents an upper bound for elastic behavior and its value, at most, is approximately an order of magnitude larger than the shear modulus: $T_y \sim 0.06$ dyn/cm. Thus, for the experiments described in the next paper (Hochmuth et al., 1982), the maximum value for the dimensionless yield will be: $\hat{T}_y = T_y/\overline{T} \sim 0.2$ since $\overline{T} \sim 0.3$ dyn/cm. If the value of $\hat{T}_y$ is significant, then there would be a discontinuity in the tether radius at the origin (Fig. 7; $\hat{V}_t \rightarrow 0$) since yield is an absolute value function. That is, if the tether velocity approaches zero through positive values, then Eq. 4 (or Eq. 10) with the addition of the yield term becomes

$$2\pi R_t^{0+}[\overline{T}(1+\hat{T}_y)] = f^{0+}, \quad V_t \rightarrow 0^+. \tag{18}$$

For a negative velocity, the limit is

$$2\pi R_t^{0-}[\overline{T}(1-\hat{T}_y)] = f^{0-}, \quad V_t \rightarrow 0^-. \tag{19}$$

The simple elastic behavior described by Eq. 14

$$f^{0+}/f^{0-} = 1/(R_t^{0+}/R_t^{0-})$$

permits Eqs. 18 and 19 to be combined:

$$R_t^{0+}/R_t^{0-} = [(1-\hat{T}_y)/(1+\hat{T}_y)]^{1/2}. \tag{20}$$

If the value for $\hat{T}_y$ is as large as 0.2, then there would be a 20% difference in the tether radius at the origin. However, the experimental results given in the next paper (Hoch-

muth et al., 1982; Figs. 7 and 9) indicate that the radius is continuous at the origin.

Even if the value for $\hat{T}_y$ is significant, the calculation of a value for the viscosity of the membrane still follows directly from Eq. 17 as long as the velocity of the tether is limited, say, to only positive values. Intuitively, this is so because in any steady-flow situation the membrane has yielded at every point on its surface. In fact, under a static condition where the elastic tether is in equilibrium with the membrane of the cell body, flow is incipient and the membrane is just on the verge of yielding. A finite yield simply adds a constant force component to the isotropic component and their sum is exactly balanced by the elastic force in the tether. An additional increase in tether force, with a concomitant decrease in tether radius, produces a flow in the cell body. Since the viscosity is calculated from derivatives of functions, an additive constant such as yield simply drops out of the equation.

To demonstrate mathematically that yield is not an important factor in the calculation of membrane viscosity, a yield term can be included in an approximate analysis similar to that given by Eqs. 7–12. Thus, Eq. 9 becomes

$$T_r = \overline{T} + T_y + \frac{2\eta V_t R_t}{r^2}, \quad V_t > 0, \qquad (21)$$

where T_y is the yield shear resultant. Eq. 10 remains unchanged while Eq. 11 becomes

$$R_t = \frac{f}{2\pi\overline{T}(1 + \hat{T}_y)} - \frac{2\eta V_t}{\overline{T}(1 + \hat{T}_y)}, \quad V_t > 0, \quad (22)$$

where $\hat{T}_y = T_y/\overline{T}$. Note that Eq. 22 reduces to Eq. 18 for $V_t \rightarrow 0^+$. Subsequent differentiation of Eq. 22, after incorporation of the correction term C, leads to the relation given by Eq. 17 since the term $(1 + \hat{T}_y)$ appears as a homogeneous term on both sides of the equation; i.e., it cancels out.

DISCUSSION

The analysis of membrane flow given in the previous section and Appendix C neglects viscous dissipation in the surrounding fluid relative to the dissipation in the membrane as membrane material flows from cell body to tether. An integration over the membrane surface area of the local rate of dissipation shows that the overall rate of dissipation in the membrane, $\dot{W}_m$, is given by

$$\dot{W}_m \sim \eta\, V_t^2$$

where η is the membrane surface viscosity and V_t is the maximum (tether) velocity. (For flow of a membrane disk, the constant of proportionality is 4π). For the bulk fluid, an integration over the volume shows that

$$\dot{W} \sim \eta_f\, V_t^2\, R$$

where $\dot{W}$ is the rate of dissipation in the bulk phase, η_f is the

bulk fluid viscosity and R is the characteristic distance, perpendicular to the membrane surface, over which significant volumetric dissipation occurs. Thus, the relative rate of dissipation is

$$\frac{\dot{W}}{\dot{W}_m} \sim \frac{\eta_f R}{\eta}.$$

A maximum value for R would be on the order of the cell radius, $R = 3\ \mu m$, and a maximum value for η_f would be the value for hemoglobin viscosity, $\eta_f = 0.1\ dyn\cdot s/cm^2$. As we will show, $\eta \sim 3 \times 10^{-3}\ dyn\cdot s/cm$. Thus, at worst,

$$\frac{\dot{W}}{\dot{W}_m} \sim \frac{10^{-1} \times 3 \times 10^{-4}}{3 \times 10^{-3}} \sim 10^{-2}$$

and the dissipation in the external bulk phase can be neglected since dissipation in the membrane is at least 100 times greater.

In addition, the analysis presented here also assumes that the viscous drag on the tether is negligible compared with the tether force f and, thus, the force (and radius) along the tether is constant. For a filament or tether drawn concentrically through a surrounding cylinder of radius R, the drag f_D on the tether is given by

$$f_D = -\eta_f\, V_t\, L_t/\ln(R/R_t),$$

where η_f is the viscosity of the surrounding fluid and V_t, L_t, R_t are tether velocity, length, and radius. In general, $\ln(R/R_t) \sim 10$ and for $V_t = 1\ \mu m/s$, $L_t = 50\ \mu m$ and $\eta_f = 0.01\ dyn\cdot s/cm^2$,

$$f_D \sim \frac{10^{-2} \cdot 10^{-4} \cdot 50 \cdot 10^{-4}}{10} \sim 5 \times 10^{-10}\ dyn,$$

which is 2,000 times smaller than the tether force f. Therefore, viscous drag on the tether can be neglected in the analysis.

In the analysis it is assumed that the membrane is very thin in comparison to the tether radius. Clearly this is only an approximation since the tether radius is ~ 200 Å or less and the membrane thickness is ~ 50 Å. Also, it is likely that a great deal of "slip" occurs between the inner and outer layer components of the membrane as the nearly planar membrane is pulled into a small cylinder with a radius <200 Å. In essence, the process of tether formation causes the inner layer to be compressed and extended from the tether into the cell body. In addition the proteinaceous inner surface of the membrane (e.g., spectrin) will also be highly deformed and compressed as it is pulled into the tether. In fact, this compressive process may be responsible for the highly viscous flow of the membrane ($\eta \sim 3 \times 10^{-3}$ dyn·s/cm) as well as the highly elastic behavior of the tether (Hochmuth et al., 1982). Future analyses should attempt to account for these various subprocesses as they occur within the overall deformation process analyzed here.

Analysis of Static Deformation

In the analysis to follow, various scaled parameters and variables are introduced. In general a bar (−) denotes a scaling with respect to the pipette radius R_p (with the exception of the isotropic tension $\overline{T}$) and a tilda (~) denotes a scaling with respect to the cell radius R_c. For example,

$$\overline{r} = \frac{r}{R_p} \qquad \tilde{r} = \frac{r}{R_c}$$

$$\overline{R}_c = \frac{R_c}{R_p} \qquad \tilde{R}_p = \frac{R_p}{R_c}$$

$$\overline{f}_w = \frac{f}{(\Delta P)_w \pi R_p^2} \qquad \tilde{f}_w = \frac{f}{(\Delta P)_w \pi R_c^2} \; ;$$

where $\Delta P_w = P_i - P_o$ (Fig. 1). Conversion from one scale to the other is accomplished by multiplying or dividing by an appropriate ratio; i.e. $\tilde{f}_w / \tilde{R}_p^2 = \overline{f}_w$. Conversion between the dimensionless wall force, $\overline{f}_w$, and the absolute force, f, is given in footnote 1:

$$\tilde{f}_w = \frac{\overline{f}}{\overline{R}_c} \frac{\overline{R}_c - 1}{\overline{R}_c - \overline{f}}, \tag{A1}$$

where $\overline{f} = f/(\Delta P)\pi R_p^2$ and $\Delta P = P_o - P_p$ (Fig. 1).

The deformed cell shown in Figs. 1 and 3 consists of three different geometric parts: (a) a cylindrical membrane with hemispherical cap, (b) a deformed but nearly spherical cell body acted on by a tether force f and a wall pressure drop $\Delta P_w = P_i - P_o$, and (c) a cylindrical tether. Deformation and displacement caused by an increase in the tether force f (with respect to ΔP_w) or an increase in the tether length will occur at constant membrane surface area and constant internal volume. The geometry of the tether and the aspirated portion of the membrane is fixed, as is the radius of the tether (Eq. 4: $\tilde{R}_t = \tilde{f}_w$). At zero tether velocity, the geometry of the membrane that encloses the cell body (Fig. 2) is specified by the equation of membrane equilibrium at constant isotropic tension (Eq. 3). However, the numerical solution for the shape of the cell body is greatly simplified when it is recognized that the spatial variable r can be expressed explicity in terms of a single independent variable, the arc-length s. Thus, all calculations for the axial distance, area, and volume are reduced to simple integration with, say, Simpson's rule.

The explicit relation between r and s is obtained by integration of

$$\frac{dr}{ds} = -\cos\theta$$

with Eq. 3 being used to eliminate $\cos\theta$:

$$\tilde{s} = (1 + \tilde{f}_w) \sin^{-1} \left(\frac{1 - \tilde{r}^2}{1 - \tilde{f}_{w}^2} \right)^{1/2} \tag{A2}$$

If necessary, Eq. A2 is readily solved for $\tilde{r}(\tilde{s})$.

The arc length from the maximum cell radius ($\tilde{r} = 1$) to the tether ($\tilde{r} = \tilde{f}_w$) is:

$$\tilde{s} = (1 + \tilde{f}_w)(\pi/2).$$

In like manner, the arc length to the pipette ($\tilde{r} = \tilde{R}_p$) can be obtained with Eq. A2.

In general, the following differential relations permit the calculation of local and overall (pipette-to-tether) axial distance z, area A and volume V:

$$dz = \sin\theta \, ds \tag{A3}$$

$$dA = 2\pi r ds \tag{A4}$$

$$dV = \pi r^2 dz = \pi r^2 \sin\theta \, ds \tag{A5}$$

where $\sin\theta$ is obtained from Eq. 3 and $r(s)$ is given by the inversion of Eq. A2.

For the situation shown in Fig. 3, the solution proceeds as follows:

(a) Pick an overall distance from the pipette to the point of attachment of the tether. In this case (Fig. 3) this distance is 15 times the pipette radius.

(b) Establish the overall surface area and volume for $\tilde{f}_w = 0$.

(c) Pick a finite $\tilde{f}_w$ and a particular cell radius $\overline{R}_c$. Obtain the overall cell-body length (Eq. A3) and the tether length (subtract the cell body length from [a], above).

(d) Calculate the volume of the cell body (Eq. A5) and the tether (since the tether radius is known: $\tilde{R}_t = \tilde{f}_w$) and then fix the extension of the membrane into the pipette so that the volume equals the fixed value given in (b) above.

(e) Finally, calculate the surface area of the cell body (Eq. A4), the tether, and the extension into the pipette (since the distance into the pipette is now given in [d] above) and sum these three values to obtain a value for the total surface area.

(f) If the surface area calculated in (e) does not agree with that given in (b), return to (c) with a new guess for the cell radius $\overline{R}_c$ and repeat the calculation until convergence to the correct surface area is obtained.

Measurement of the Radius of a Tether Extracted from a Spherical Cell Body

For small tether forces, the cell body will be spherically shaped as shown by Eq. 3 and Fig. 3 A and B. In this case, the total surface area of the cell membrane and the volume enclosed by the membrane are

$$A = \underbrace{2\pi R_p L_p}_{\text{pipette}} + \underbrace{4\pi R_c^2 - \pi R_p^2}_{\text{cell body}} + \underbrace{2\pi R_t L_t}_{\text{tether}} \tag{B1}$$

$$V = \underbrace{\tfrac{1}{3}\pi R_p^3 + \pi R_p^2 L_p +}_{} \underbrace{\tfrac{4}{3}\pi R_c^3}_{} + \underbrace{\pi R_t^2 L_t}_{}. \tag{B2}$$

R and L denote radius and length and the subscripts p, c, and t denote pipette, cell, and tether. The derivatives with respect to L_t of Eqs. B1 and B2 at constant area and volume give

$$2\pi R_p \frac{dL_p}{dL_t} + 8\pi R_c \frac{dR_c}{dL_t} + 2\pi R_t = 0 \tag{B3}$$

$$\pi R_p^2 \frac{dL_p}{dL_t} + 4\pi R_c^2 \frac{dR_c}{dL_t} + \pi R_t^2 = 0. \tag{B4}$$

The elimination of dR_c/dL_t between Eqs. B3 and B4 gives

$$R_t = \left(1 - \frac{R_p}{R_c} \right) \cdot R_p \left(-\frac{dL_p}{dL_t} \right), \tag{B5}$$

which is Eq. 6 in the text. In like manner, an expression for the change in cell radius with tether length can be obtained:

$$\frac{dR_c}{dL_t} = \frac{1}{4} \left(\frac{R_t}{R_c} \right) \left(\frac{R_p/R_c}{1 - R_p/R_c} \right), \tag{B6}$$

where the approximation $1 - R_t/R_p = 1$ has been made. Eq. B6 shows that the change in cell radius with cell length is negligible. For example, typical values for the geometric ratios in Eq. B6 give

$$\frac{dR_c}{dL_t} = \frac{1}{4} \frac{0.02}{3} \frac{1/3}{1 - 1/3} \approx 10^{-3}.$$

Thus an increase in tether length of 50 μm results in an increase in cell radius of only ~0.05 μm.

It is interesting to compare an actual calculation obtained from the analysis of static deformation (Appendix A) to the slope predicted by Eq. B5. Thus, when Eq. B5 is rearranged together with the relations given by Eq. 4 ($\bar{R}f = \bar{f}_w$) and footnote 1, the following expression is obtained:

$$-\frac{dL_p}{dL_t} = \bar{f}\left[\frac{\bar{R}_c}{\bar{R}_c - \bar{f}}\right]. \qquad (B7)$$

When $\bar{f} = 0.15$ and $\bar{R}_c = 4$, Eq. B6 predicts

$$-\frac{dL_p}{dL_t} = 0.156.$$

A numerical integration similar to the one discussed in Appendix A gives

$$-\frac{dL_p}{dL_t} = 0.148,$$

which indicates only a negligible error (~5%) when Eq. B5, based on a spherical cell body, is used to calculate tether radius.

APPENDIX C

Analysis of Continuous Axisymmetric Flow

When $V_t = 0$ (V_t = tether velocity), the equation of membrane equilibrium along the meridian indicates that $\bar{T}$ = constant. When membrane flow occurs from cell body to tether, the equations of membrane equilibrium are still applicable although the flow itself causes a deviation from the isotropic state. Thus, the axial force balance (see Eq. 1 and Fig. 3) and the equation of membrane equilibrium along the meridian (Flugge, 1973; Evans and Hochmuth, 1976) are

$$T_m \cdot 2\pi r \sin \theta = (\Delta P)_w \pi r^2 + f \qquad (C1)$$

$$r\frac{dT_m}{ds} + (T_m - T_\phi)\frac{dr}{ds} = 0, \qquad (C2)$$

where T_m is the principal force resultant (force per unit length) in the meridional direction and T_ϕ is the resultant in the circumferential direction. It is interesting to note that the derivative of Eq. C1 with respect to r, when combined with Eq. C2, readily yields the law of Laplace,

$$\frac{T_\phi}{R_\phi} + \frac{T_m}{R_m} = (\Delta P)_w$$

with $R_\phi = \sin \theta/r$, $R_m = ds/d\theta$ and $\cos \theta(dr/ds) = 1$ (see Fig. 3). Thus, Eqs. C1 and C2 implicitly contain the law of Laplace.

Newton's law of viscosity expressed in terms of the shear resultant, $(T_m - T_\phi)/2$, is

$$\frac{T_m - T_\phi}{2} = 2\eta \frac{dv_s}{ds} \qquad (C3)$$

where v_s is the velocity along the meridian s and η is the coefficient of surface viscosity. The equation of continuity (conservation of mass) is

$$v_s = \frac{R_t V_t}{r} \qquad (C4)$$

since $2\pi r v_s$ = constant.

The combination of Eqs. C2–C4 along with the differential geometric relation,

$$\frac{dr}{ds} = -\cos \theta, \qquad (C5)$$

immediately yields

$$\frac{dT_m}{ds} = 4\eta \frac{R_t V_t}{r^3} \cos^2 \theta. \qquad (C6)$$

If the geometry of the surface is specified (e.g., a flat surface with $\theta = 0$ and $ds = -dr$), then this equation is readily integrated.

The division of both sides of Eq. C1 by $2\pi r$ and differentiation of the result with respect to r yields

$$T_m \cos \theta \frac{d\theta}{dr} + \sin \theta \frac{dT_m}{dr} = \frac{(\Delta P)_w}{2} - \frac{f}{2\pi r^2}. \qquad (C7)$$

The substitutions of dr from Eq. C5, dT_m/ds from Eq. C6 and T_m from Eq. C1 yield, after some rearrangment,

$$-\frac{d\theta}{d\tilde{s}} = \frac{8\eta R_t V_t}{R_c^3(\Delta P)_w} \cdot \frac{\sin^2 \theta \cos \theta}{\tilde{r}^3(\tilde{r} + \tilde{f}_w/\tilde{r})}$$
$$+ \frac{(1 - \tilde{f}_w/\tilde{r}^2) \sin \theta}{(\tilde{r} + \tilde{f}_w/\tilde{r})} \qquad (C8)$$

where $\tilde{r} = r/R_c$, $\tilde{s} = s/R_c$, $\tilde{f}_w = f/(\Delta P)_w \pi R_c^2$ and $\Delta P_w = P_i - P_o$. The first term in Eq. C8 represents the effect of flow on the shape of the membrane while the second term represents the static shape ($V_t \rightarrow 0$, see Eq. 1).

The results from the simple disk-flow analysis (Eq. 11) leads to a natural "scale" for the coefficient which multiplies the first term in Eq. C8. To this end, Eq. 11 is scaled with respect to the tether radius at zero velocity; i.e., $R_t \rightarrow R_t^0$ and $f \rightarrow f^0 = 2\pi \bar{T} R_t^0$ as $V_t \rightarrow 0$:

$$\hat{R}_t = \hat{f} - \hat{V}_t \qquad (C9)$$

where $\hat{R}_t = R_t/R_t^0$, $\hat{f} = f/f^0$ and $\hat{V}_t = 2\eta V_t/R_t^0 \bar{T}$. Just as the bar ($-$) denotes scaling with respect to the pipette radius R_p and the tilda ($\sim$) denotes scaling with respect to the cell radius R_c, the circumflex (^) denotes scaling with respect to the tether radius at zero velocity, R_t^0. For various fixed values of $\hat{f}$, Eq. C9 represents a series of parallel lines with $-45°$ slopes. However, only a single point on any particular line represents the experimental situation (e.g., $\hat{R} = 1$ at $\hat{f} = 1$ and $\hat{V}_t = 0$).

When scaled with respect to R_t^0, the first-term coefficient in Eq. C8 becomes

$$\frac{8\eta R_t V_t}{R_c^3(\Delta P)_w} = \frac{4\eta R_t V_t}{\bar{T} R_c^2} = 2(\tilde{R}_t^0)^2 \hat{R}_t \hat{V}_t = (\tilde{R}_t^0)^2 \hat{Q}_t$$

where $\tilde{R}_t^0 = R_t^0/R_c$ and $\hat{Q}_t = 2\hat{R}_t \hat{V}_t$. The dimensionless force term in Eq. C8, $\tilde{f}_w$, can also be rescaled with respect to R_t^0:

$$\tilde{f}_w = \tilde{R}_t^0 \hat{f}$$

where $\hat{f} = f/2\pi R_t^0 \bar{T}$. Thus, Eq. C8 is rewritten as

$$-\frac{d\theta}{d\tilde{s}} = \frac{(\tilde{R}_t^0)^2 \hat{Q}_t \sin^2 \theta \cos \theta}{\tilde{r}^3(\tilde{r} + \tilde{R}_t^0 \hat{f}/\tilde{r})} + \frac{(1 - \tilde{R}_t^0 \hat{f}/\tilde{r}^2) \sin \theta}{\tilde{r} + \tilde{R}_t^0 \hat{f}/\tilde{r}}. \qquad (C10)$$

Also,

$$\frac{d\tilde{r}}{d\tilde{s}} = -\cos \theta. \qquad (C11)$$

In order to accomplish the simultaneous integration of Eqs. C10 and C11, an initial value is assigned to $\tilde{R}_t^0$ ($\tilde{R}_t^0 = R_t^0/R_c = 0.01, 0.005$, etc.).

However, the result will be essentially independent of the particular value for $\hat{R}_t^0$ as long as $\hat{R}_t^0$ is small since in this case the only characteristic dimension in the problem is the tether radius (Eq. 11). With a fixed value for $\tilde{R}_t^0$ and a fixed value for $\hat{f}$ (e.g., 0.5, 1, 1.5), a particular value is assigned to $\hat{Q}_t$ and a forth-order Runga-Kutta algorithm is used to simultaneously integrate Eqs. C10 and C11 between the limits $\theta = \pi/2$, $\tilde{r} = 1$ and $\theta = \pi/2, \tilde{r} = \tilde{R}_t = R_t/R_c$. That is, the membrane material turns the corner and forms a tether when $\theta \rightarrow \pi/2$ for the second time. Once the value for $\tilde{R}_t$ is established at $\theta = \pi/2$, the values for $\hat{V}_t$ and $\hat{R}_t$ are calculated:

$$\hat{R}_t = \frac{\tilde{R}_t}{\tilde{R}_t^0}, \qquad \hat{V}_t = \frac{\hat{Q}_t}{2\tilde{R}_t}.$$

In this way, graphs of $\hat{R}_t$ vs. $\hat{V}_t$ at constant f can be created from the integration of Eqs. C10 and C11. The results of this procedure are shown in Fig. 7 in the text. Note that the actual slope of the plot of $\hat{R}_t$ vs. $\hat{V}_t$ is somewhat shallower than the $-45°$ slope predicted by Eq. C9. At the origin the curve has a slope of $-1/1.6$. Thus, Eq. C9 is modified accordingly

$$\hat{R}_t = \hat{f} - \hat{V}_t/C \qquad (C12)$$

where $C = 1.6$. This equation appears in the text as Eq. 13. In dimensional form Eq. C12 is written as

$$R_t = \frac{f}{2\pi\bar{T}} - \frac{2\eta V_t}{C\bar{T}}. \qquad (C13)$$

H. Craig Wiles provided the photograph shown in Fig. 4. Leigh Smith performed the numerical calculations for Figs. 7–9. We gratefully acknowledge their contributions.

REFERENCES

Evans, E. A. 1973. New membrane concept applied to the analysis of fluid shear- and micropipettet-deformed red blood cells. *Biophys. J.* 13:941–954.

Evans, E. A., R. Waugh, and L. Melnik. 1976. Elastic area compressibility modulus of red cell membrane. *Biophys. J.* 16:585–595.

Evans, E. A., and R. M. Hochmuth. 1976. Membrane viscoplastic flow. *Biophys. J.* 16:13–26.

Flugge, W. 1973. Stresses in Shells. Springer-Verlag New York Inc., New York.

Hochmuth, R. M., N. Mohandas, and P. L. Blackshear, Jr. 1973. Measurement of the elastic modulus for red cell membrane using a fluid mechanical technique. *Biophys. J.* 13:747–762.

Hochmuth, R. M., E. A. Evans, and D. F. Colvard. 1976. Viscosity of human red cell membrane in plastic flow. *Microvasc. Res.* 11:155–159.

Hochmuth, R. M., H. C. Wiles, E. A. Evans, and J. T. McCown. 1982. Extensional flow of erythrocyte membrane from cell body to elastic tether. II. Experiment. *Biophys. J.* 38:83–89.

Rand, R. P., and A. C. Burton. 1964. Mechanical properties of the red cell membrane. I. Membrane stiffness and intracellular pressure. *Biophys. J.* 4:115–135.

Waugh, R., and E. A. Evans. 1979. Thermoelasticity of red blood cell membrane. *Biophys. J.* 26:115–131.